Reaction and total cross sections for 400–500 MeV π^- on nuclei

C. J. Gelderloos,* J. T. Brack, M. D. Holcomb,† M. V. Keilman,‡ D. J. Mercer,§ R. J. Peterson, R. A. Ristinen, and A. Saunders§

Nuclear Physics Laboratory, University of Colorado, Boulder, Colorado 80309-0446

(Received 6 March 2000; published 21 July 2000)

Attenuation measurements of reaction and total cross sections have been made for π^- beams at 410, 464, and 492 MeV on targets of CD_2, ^{6}Li, C, Al, S, Ca, Cu, Zr, Sn, and Pb. These results are assisted by and compared to predictions from a recent eikonal optical model. Calculations with this model, which does not include pion absorption, agree with recent elastic scattering data, but are significantly below our measured reaction and total cross sections.

PACS number(s): 25.80.Hp

I. INTRODUCTION

In describing interactions between pions and nuclei, there are two primary observables by which reaction models can be evaluated: differential elastic cross sections and integrated total and total reaction cross sections. Measurements of elastic cross sections are useful for extracting optical model parameters and are the most common observable for pion energies below 300 MeV. As the beam momentum of the pion increases, however, measurements of elastic cross sections become more difficult, since the absolute energy resolution of the scattered pion becomes poorer; only for a few nuclei may the elastic peak be cleanly resolved. Additional observables to constrain reaction models are the total and reaction cross sections, but their determination from beam transmission measurements is coupled intimately with models for the differential elastic cross sections, as treated in detail below.

At pion beam energies above 300 MeV there have been recent data for elastic scattering on carbon, silicon, calcium, zirconium, and lead [1–4]. Another recent development for this pion energy range is a new reaction model based upon an eikonal method, removing the need to limit the partial waves to be considered [5]. The recent elastic data may serve to verify that reaction model, which may then be used as a vital ingredient for the evaluation of total and reaction cross sections, which in turn serve as further tests of the model. This model and its tests by elastic scattering were not available for previous analyses of pion-nucleus total and reaction cross sections above 300 MeV [6–8]. We have thus carried out a new experiment, with several technical advances over previous procedures and a new model analysis for the required corrections, to measure these observables for pion beams between 400 and 500 MeV, using a wider range of nuclear samples than could be used for elastic scattering studies.

At the higher beam energies used for these studies, the wavelength of the pion projectile is shorter than mean internucleon spacings, and the small π-N cross sections give much better access to the nuclear interior than is the case at resonance energies. This leads to the hope that medium modifications or alterations of N^* within nuclei [9,10] may be found at the higher energies.

The present pion results, at 479, 588, and 616 MeV/c, are also valuable for comparison to recent K^+-nucleus total and reaction cross sections for 488 to 714 MeV/c [11], where reaction models are also tested by comparison to recent elastic scattering data [12]. The wavelengths of these beams are also short enough to sense the properties of individual nucleons within complex nuclei, and the spin/isospin couplings of π and K^+ mesons to nucleons are very similar [13]. A K^+ has a long mean free path, and may sense medium effects at high nuclear density, while the pion is restricted to interactions in the nuclear surface. The elementary K^+-nucleon coupling in this momentum range is almost entirely elastic, while the inelastic part of the π-nucleon interaction, averaged over a symmetric nucleus, increases from 19% at 410 MeV to 39% at 492 MeV. The π may also be absorbed in complex nuclei, while this does not occur for K^+. We may anticipate from these similarities and differences that comparison of data with K^+ and pions will be of great interest.

The transmission technique used in the present work is very similar to that employed for many previous measurements of total and reaction cross sections. The improvements we have made to permit better systematic uncertainties are based upon the high beam intensities available at LAMPF, which permitted a simpler experimental setup. Of equal importance is the use of the new optical model code to make corrections to extract the desired data from changes in the transmission of the pion beams through our targets. We demonstrate the validity of these methods by comparisons of examples of pion elastic scattering data across our energy range to the predictions of the eikonal DWIA code [5], establishing its reliability. The good agreement found for these cases leads to confidence in the use of the eikonal optical model to make the corrections needed to obtain accurate and robust total and reaction cross sections for a wide range of nuclear masses. We also explored several optical model variations to establish a systematic uncertainty for our results.

*Present address: Hughes Space and Communications Company, MS S25/C369, P.O. Box 92919, Los Angeles, CA 90009.

†Present address: Honeywell, Chippewa Falls, WI 54729.

‡Present address: 1420 Bluebell Ave., Boulder, CO 80302.

§Present address: Los Alamos National Laboratory, Los Alamos NM 87544.

 ©2000 The American Physical Society

TABLE I. Detector dimensions and positions relative to the beam pipe exit.

Detector	Diameter (cm)	Thickness (mm)	Distance from beam pipe exit (cm)
$S1$	1.0	3.2	206.5
$S2$	1.5	1.6	343.7
$S3$	1.0	1.6	347.2
Target	$\sim$5.0	$\sim$10	350.9
$S4_{\min}$	15.0	6.35	434.6
$S5$	5.0	3.2	$S4+2.0$

II. EXPERIMENTAL METHODS

The measurement of a transmission cross section consists of determining the cross section for scattering the projectile outside of some solid angle Ω. In order to determine the transmission cross section at zero solid angle, which is the quantity of interest, the measurement is performed at several solid angle settings, and then extrapolated to zero solid angle.

The P^3 channel at the former Los Alamos Meson Physics Facility (LAMPF) was used for the pion source [14]. The setup consisted of a series of three aligned scintillation detectors upstream of the target, functioning as a beam telescope to define a narrow collimated negative beam incident on the target. Pion kinetic energies were 410, 464, and 492 MeV at the center of a typical target, with an uncertainty of less than 1% and a momentum spread of 0.2%. Beam energies of the incident pions were determined by time of flight and comparison to recent calibration measurements using proton time of flight [15].

Muon contamination of the beam was less than 0.5%, and electrons in the beam were excluded from the trigger by their timing. The beam defining telescope was used to select a beam spot 1.05 cm in diameter at the target, with an angular divergence of less than 7 mrad. Table I lists the elements of this telescope, with a trigger of $S1\times S2\times S3$ required. No anticoincidence system was used. Average incident beam trigger intensities ranged from 5000 to 6500 π/sec, and the duty factor of the beam was 6.1%.

Targets were as listed in Table II, and were significantly thinner than those of previous works [8]. The CD_2 target includes a 3.4% impurity of CH_2 by weight. The ^{6}Li and Ca targets were clad in thin aluminum foil. All target thicknesses were known to within 1%, save for ^{6}Li. Corrections for the cladding and for the C and H content of the CD_2 target were made.

Downstream of the target was the transmission counter, mounted on a moveable platform so that its solid angle could be changed from run to run. A fifth scintillator was mounted directly behind the transmission counter to determine the efficiency of the transmission counter. Detector dimensions and thicknesses are listed in Table I.

Analog signals from the detectors were passed to the counting house, where both ADC and TDC signals were recorded on 8 mm magnetic tape for offline analysis. Trigger conditions included a triple coincidence between the three telescope scintillators upstream of the target, such that beam pions were collimated by definition.

Corrections for the efficiency of the transmission counter ($S4$) were made run-by-run; observed inefficiencies were never worse than 1 part in 10 000, and known to better than that. Solid angles of the transmission counter were measured geometrically to within 1%. Eight solid angles were used for each target and beam energy. The solid angles in msr were 596, 499, 394, 298, 201, 149, 101, and 25.0, achieving lower values and thus less extrapolation than in Ref. [8].

Beam rates were limited by an acceptable electronic live time in the data acquisition system, which was typically 80–90 % and known to within 2%. Dead time corrections were unnecessary in data analysis, as the transmission cross section is calculated from a ratio of detected beam pions to scattered pions and data rates were almost identical with and without a target.

The attenuation cross section of a pion beam through a target of N atoms/cm^2 can be defined as

$$\sigma_{\text{atten}}(\Omega)=\frac{1}{N}\ln\left[\frac{B_i}{T_i}\frac{T_o}{B_o}\right]=\sigma_R(\Omega)+\sigma_{\text{EC}}(\Omega), \qquad (1)$$

TABLE II. Targets and their thicknesses, most known to 1%. Geometrical parameters as listed were used for neutron and proton distributions in the optical model calculations. Fermi distributions were derived from charge distributions [19] with the nucleon sizes removed by convolution. [20] Harmonic oscillator parameters are from Ref. [11], used there for K^+ reaction and total cross sections.

Target	model	c(fm)	a(fm)	w	Rad. lengths	Thickness (g/cm^2)
CD_2					0.0253	1.439
^{6}Li	SHO	$c=1.77$ fm, $z=0.327$			0.0054	0.4484
C	SHO	$c=1.516$ fm, $z=2.234$			0.0407	1.737
Al	$2pf$	3.013	0.491		0.111	2.665
S	$3pG$	2.609	2.069	0.205	0.0049	1.011
Ca	$3pf$	3.787	0.485	-0.139	0.087	1.553
Cu	$2pf$	4.292	0.498		0.120	1.540
Zr	$2pf$	4.737	0.530		0.196	2.105
Sn	$2pf$	5.488	0.454		0.133	1.173
Pb	$2pf$	6.583	0.506		0.117	0.744

where B_i (B_o) and T_i (T_o) are the number of detected beam and transmitted pions with the target in (out), respectively. This attenuation cross section is comprised of a reaction cross section $\sigma_R(\Omega)$ and an elastic scattering cross section $\sigma_{\rm EC}(\Omega)$ beyond the solid angle Ω of the detector. Each elastic cross section $\sigma_{\rm EC}$ can be written as

$$\sigma_{\rm EC}(\Omega)=\sigma_{\rm el}(\Omega)+\sigma_C(\Omega)+\sigma_{\rm NCI}(\Omega), \qquad (2)$$

comprised of contributions from nuclear elastic $\sigma_{\rm el}$, Coulomb σ_C, and nuclear-Coulomb interference $\sigma_{\rm NCI}$. The reaction cross section $\sigma_R(\Omega)$ is calculated by subtracting the elastic scattering component at each of eight solid angle settings for the transmission counter and extrapolating to $\Omega=0$.

III. ANALYSIS

Whatever corrections could be reasonably and safely made online were done so at the time of the experiment. Those corrections that were unaddressable during the experiment were made offline in software. Expected corrections to which there was no reasonable access were modelled in Monte Carlo fashion, and the necessary corrections were applied. Finally, elastic corrections were made through the use of a calculational model. Each of these steps is discussed in more detail below.

In offline analysis, a series of restrictive cuts were made on the taped data. Since adequate numbers of events were collected for all configurations, we were able to be selective in determining a valid threefold beam coincidence. Cuts on the data included cutting out events which reacted in any of the scintillators upstream of the target or $S4$, cutting out beam doubles in which more than one pion was detected during a single trigger, time-of-flight cuts to eliminate beam contaminants such as electrons, narrow time gates such that only pions within the same 5 ns microburst of the LAMPF beam time structure were accepted, and efficiency corrections based on comparisons of count rates in the transmission counter ($S4$) and $S5$. Identical cuts and tests were applied to runs with and without a target.

In addition to the offline corrections, there remained several possible sources of systematic error that could not be experimentally measured. To correct for these effects a Monte Carlo simulation based on GEANT was used to calculate additional correction factors. Details that were included in the Monte Carlo simulations include corrections for residual muon contamination in the beam, pion decay both before and after the target, recoil protons that could not be eliminated in software cuts, delta rays in the transmission counter, multiple scattering in the target, plural or Moliere scattering to angles at the edges of the transmission counter, and pion production. Elastic cross sections as described below were used in GEANT for full consistency.

The dominant Monte Carlo corrections were for pion decay and plural scattering. Pion decay can lead to scattered events that appear to be unscattered, or unscattered events that appear to be scattered. (For any given solid angle configuration, we define a scattered event to be one in which the pion is scattered to a polar angle outside of that of the transmission counter.) To first order, these two effects should cancel, as is confirmed by Monte Carlo methods. Higher order effects are small, about 0.5%. Whenever the angular distribution is changing rapidly over the angles of interest, as is the case at small angles, the effects of plural scattering can be significant. For example, since there are more scattered pions at smaller angles than larger, there tend to be more summed experimental events in which smaller angles become larger due to plural scattering than those in which larger angles become smaller, simply because of the initial number of events at smaller and larger angles. These corrections are not large in the Monte Carlo, but become very important in the elastic subtraction process, described below.

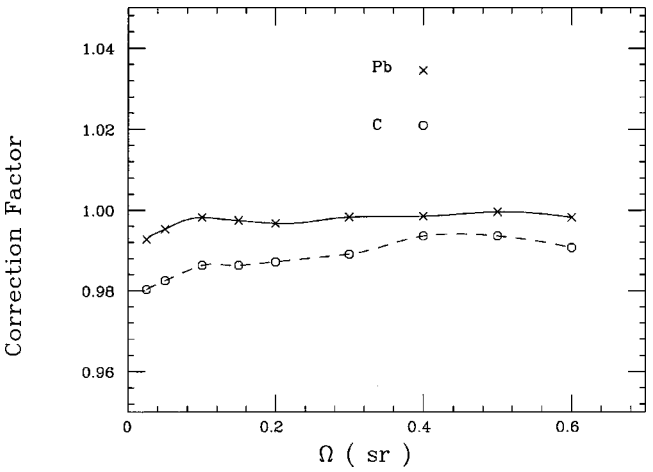

FIG. 1. Computed Monte Carlo correction factors are shown, used to modify the measured attenuation cross sections before further analysis at 410 MeV. Effects included in this modeling are described in the text. The lead example is for a target 0.74 gm/cm^2 thick and the carbon target was 1.74 gm/cm^2 thick.

Pion production, although increasing significantly over the range of energies measured in this experiment, does not affect the final cross sections, as it disappears in the extrapolation to zero solid angle. Protons from the targets also give a yield that extrapolates to zero.

Overall Monte Carlo corrections were less than 2% for all target and beam energies. Half of these corrections are included in the quoted uncertainties. Samples are shown in Fig. 1.

The next step in the analysis path was to subtract the elastic component $\sigma_{\rm EC}(\Omega)$ of the scattering from the attenuation cross sections. For the majority of targets the elastic corrections were calculated using the code of Chen *et al.* [5]. This eikonal-based code was first checked against existing elastic differential cross section measurements. The distribution of nucleon centers was determined by unfolding them from charge distributions. Modified two- and three-parameter Fermi parameters, harmonic oscillator formulations, or three-parameter Gaussian parameters were used to describe the distribution of nuclear centers, as shown in Table II [20]. For carbon, nucleon distributions were also used as calculated independently by Chen [5] and Friedman [11]; this enabled us to determine another systematic uncer-

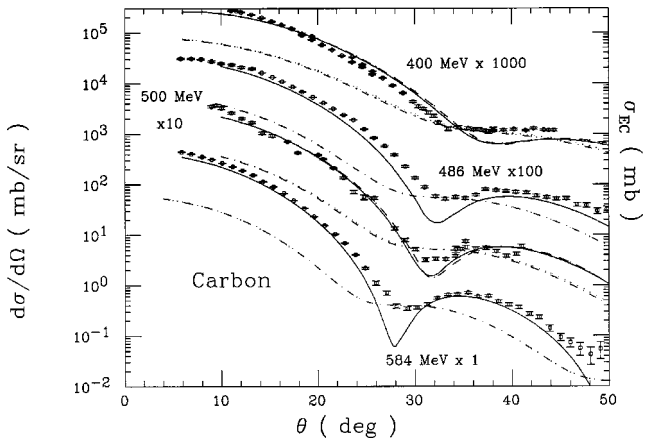

FIG. 2. Examples of how our optical model calculations agree with measured elastic differental cross section data for carbon. Solid lines use the parameters listed in Table II and dashed lines for 400 and 500 MeV use the Hartree-Fock distributions of Ref. [5]. The dot-dashed curves show the computed σ_{EC} with the parameters of Table II, used to analyze our attenuation data to obtain reaction cross sections. The dotted curves for 400 and 500 MeV use the distribution of Ref. [5]. The two matter distributions yield almost identical results. Data at 400 and 500 MeV are from Ref. [2], while 486 and 584 MeV data are from Ref. [1]. Differential cross section results use the left scale and the center of mass angles. Elastic correction curves use the right scale, with the same numerical scale as the left, and laboratory frame angles.

tainty. For deuteron corrections, differential cross sections were calculated by Garcilazo [16]. Samples of these computed cross sections are compared to data in Figs. 2 and 3.

Differential cross sections for each target of the present work were calculated and integrated over each solid angle, after having been convoluted with the plural scattering distribution, to yield $\sigma_{EC}(\Omega)$. The effects of including the effects of plural scattering were significant due to the steepness of the elastic cross section. The difference between an assumed Gaussian approximation for multiple scattering and

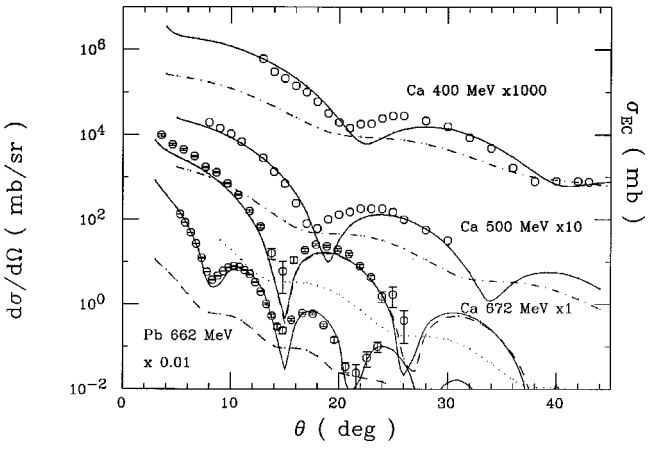

FIG. 3. Examples of elastic π^- scattering from heavier nuclei are shown, comparing data from Ref. [1] for ^{208}Pb, from Ref. [4] for Ca at 672 MeV, and Ref. [2] for Ca at 400 and 500 MeV. Computed elastic cross sections and elastic correction cross sections are shown as in Fig. 2.

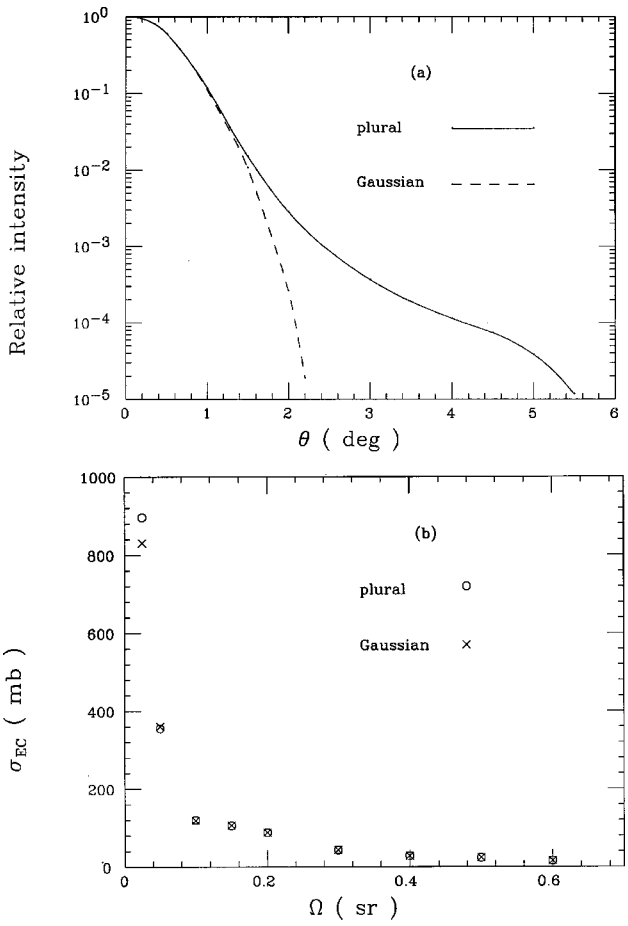

FIG. 4. A pion beam particle suffers small angle scattering before and after a nuclear scattering event, such as is calculated by an optical model. This figure shows the relative effect of Gaussian and plural scattering on these trajectories. Monte Carlo corrections and final σ_{EC} used the plural scattering distributions to model those contributions to our attenuation data. The example shown is for lead at 410 MeV. Effects of Gaussian or plural scattering as shown in the lower panel are shown for elastic corrections to the attenuation data.

that including plural scattering is shown in Fig. 4 for our worst case, which includes cross sections even steeper than those considered in Ref. [17]. Samples of our σ_{EC} are shown in Figs. 2 and 3, before convoluting.

In the case of the CD_2 target, the carbon component had to be explicitly subtracted from the CD_2 attenuation cross sections. We also used known πp cross sections [23] to correct for the small H contamination in the CD_2 targets.

The calcium target had increased from its original mass at the time of the experiment. Cross sections for Ca were determined by assuming contaminants of CaO or $Ca(OH)_2$, with the results averaged. Differential elastic cross sections from the contaminants were included, as were the attenuation cross sections for oxygen. These were determined by interpolation, with an assumed 5% uncertainty. Half the difference between attenuation cross sections with the two assumptions was added as an uncertainty before extrapolating these to $\Omega = 0$.

The ^{6}Li target had also increased its original mass when

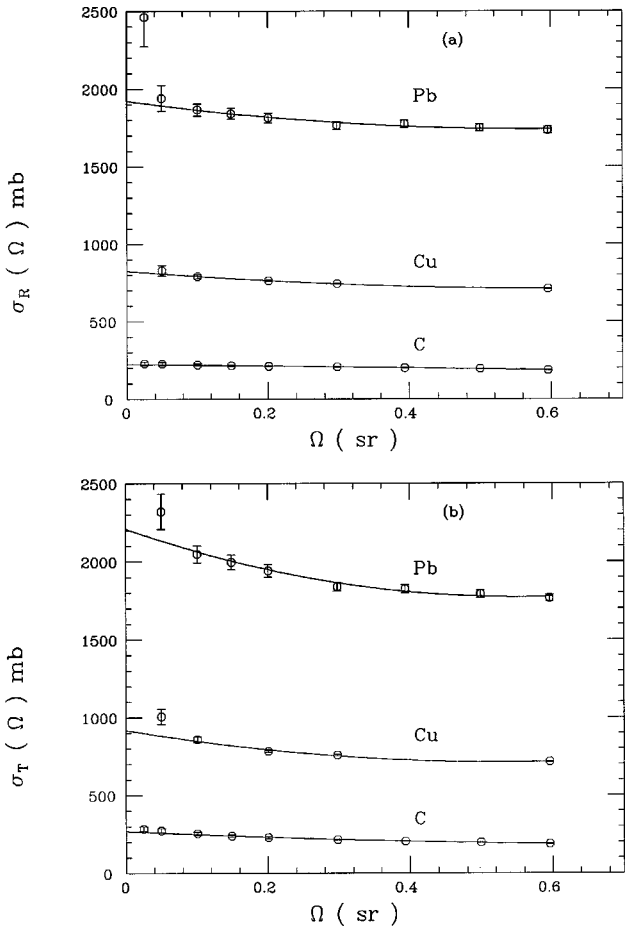

FIG. 5. Samples of the quadratic extrapolation used to obtain reaction and total cross sections. The lead case is for 410 MeV, the copper for 464 MeV, and the carbon for 492 MeV.

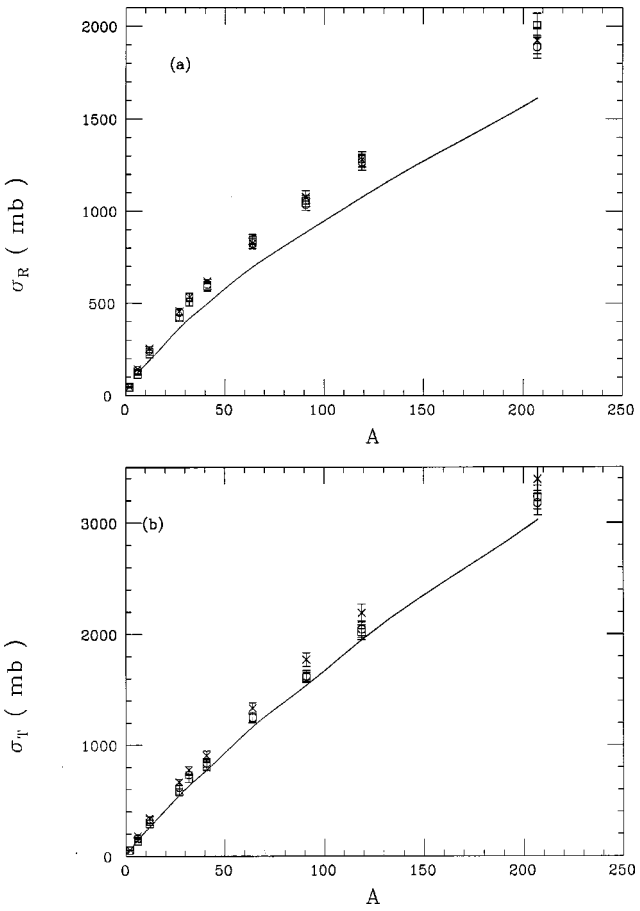

FIG. 6. Shown are the three reaction and total cross section data sets for our beam energies of 410 MeV (crosses), 464 MeV (circles), and 492 MeV (squares). The curves are those computed from the optical model of Ref. [5] at the middle energy of 464 MeV.

the experiment was carried out. We assumed contaminations of either $^6Li_2O$ or ^6LiOH to compute attenuation cross sections, similar to the method used for calcium. A 2% uncertainty for the original and final masses was used. Half the difference between the two methods used to obtain the attenuation cross sections was used as an uncertainty.

After correcting each attenuation cross section for elastic scattering, a least-squares-fitting procedure was used to extrapolate to zero solid angle. For the heaviest targets, it became obvious that even the detailed corrections for plural scattering were insufficient to account for small angle processes. In such cases where the smallest solid angle measurement lay more than two standard deviations away from the least-squares fit results, that cross section was excluded from the extrapolation process. Sample extrapolations are shown in Fig. 5.

Systematic uncertainties due to the extrapolation to zero solid angle were estimated by determining the difference in reaction cross section between linear, quadratic, and cubic fitting polynomials. These uncertainties were about 2–5%. In nearly all cases, a quadratic fit yielded the lowest chi-squared value; quadratic fits were therefore used for all targets and energies, for final results shown in Fig. 6 and listed in Table III for all targets.

Checks for other sources of systematic uncertainty were made by varying target thickness and beam rates for some targets during the experiment. All results were consistent within statistical uncertainties after Monte Carlo corrections.

Determination of the total cross section was done following the procedure outlined in Ref. [18]. In essence, the nuclear elastic cross-section was added to the extrapolated reaction cross sections for each target for each Ω. The nuclear elastic cross sections were calculated using the eikonal code [5] with the Coulomb force not calculated. The incident pion energies were adjusted slightly to compensate for the Coulomb energy. The resulting $\sigma_T(\Omega)$ were extrapolated quadratically to $\Omega=0$ as shown in Fig. 5, to yield the total cross sections listed in Table IV and plotted in Fig. 6.

IV. SYSTEMATIC UNCERTAINTIES

Statistical uncertainties from all sources were small, never more than 0.1% of the final σ_R or σ_T. Sources of the more important systematic uncertainties were explored in detail. Those corrections which could not be made by software cuts were studied via Monte Carlo simulations, as described previously. Calculated Monte Carlo corrections were less than

TABLE III. Reaction cross sections in mb obtained in the present work. The first number in parentheses is the uncertainty from causes listed in the text, and the second uncertainty results from including the uncertainty in the normalization of the elastic scattering data we use to verify the optical model calculations used for the elastic corrections, when available. Figures shown use the first uncertainty.

Pion Ke (MeV)	^{2}H	^{6}Li	C	Al	S
410	46.9(2.6)	143(13)	255(11)(15)	456(23)(26)	533(27)(24)
464	43.5(2.3)	137(16)	244(10)(14)	451(27)(44)	534(24)(27)
492	45.2(2.5)	113(7)	224(9)(12)	420(24)(29)	507(43)(72)
	Ca	Cu	Zr	Sn	Pb
410	618(26)(85)	827(35)(37)	1078(44)(46)	1280(53)(55)	1922(90)(95)
464	602(36)(80)	825(36)(42)	1037(32)(34)	1266(65)(78)	1888(86)(90)
492	592(32)(74)	847(34)(35)	1057(38)(40)	1283(140)(142)	2005(140)(236)

2% for all targets and beam energies; half of these corrections were included in the stated uncertainties for the final cross sections.

Sources of systematic uncertainty in the subtraction of the elastic scattering component were primarily the uncertainty in the parameters describing the distribution of nucleons in the nuclei, and the method of extrapolation to zero solid angle. Systematic uncertainties due to the elastic corrections were evaluated by numerically differentiating with respect to the parameters of the Fermi or Gaussian nucleon distribution functions and using the quoted uncertainties in those parameters [19]. Since these corrections were not independent of the solid angle of the transmission counter, systematic uncertainties were calculated for each solid angle and included before extrapolating to zero solid angle. We used two nucleon distributions for carbon as our example. The Hartree-Fock [5] and harmonic oscillator [11] models gave σ_{EC} results differing by 0.5% at most. These are shown in Fig. 2.

A systematic uncertainty harder to assess is the reliability of the elastic scattering calculations used for σ_{EC} and σ_{el}. Measured elastic cross sections have stated uncertainies in normalization of 10% [1], 16% [2], 12% [3], and 15% [4]; these error bars are not shown in the data in Figs. 2 and 3. In addition, an angular uncertainty of 0.84° is cited in Ref. [2]. For carbon, a 10% decrease in elastic calculations in the forward cross sections would increase σ_R by about 1% and σ_T by about 3%.

Comparisons in Figs. 2 and 3 show cases of calculations below the elastic data by about 15% in some cases. For many of the heavy targets studied at 400 and 500 MeV in Ref. [2], similar calculations are far from agreement with the data. Nonetheless, we used the model of Ref. [5] to compute σ_{EC} and σ_{el} for these cases as well. It is to be noted in Fig. 3 that all data for targets heavier than carbon other than those from Ref. [2] are in good agreement with the calculations. Data from Ref. [2] are not matched by the calculations in many cases.

In order to estimate an additional systematic uncertainty due to our inability to guarantee agreement with elastic data, we also include in Tables III and IV the uncertainties that result from propagating the stated normalization uncertainties from experiments nearest our cases. These are sometimes much larger than the uncertainties, also listed, resulting directly from our measurements.

V. RESULTS AND DISCUSSION

Reaction and total cross sections obtained from the present experiment are listed in Tables III and IV. Uncertain-

TABLE IV. Total cross sections in mb obtained in the present work. Uncertainties are shown as in Table III.

Pion Ke (MeV)	^{2}H	^{6}Li	C	Al	S
410	58.6(3.0)	180(14)	341(16)(20)	664(30)(41)	774(36)(44)
464	52.1(2.6)	160(16)	314(14)(18)	621(32)(51)	732(30)(40)
492	52.8(2.8)	134(7)	290(13)(16)	580(28)(38)	696(50)(77)
	Ca	Cu	Zr	Sn	Pb
410	905(44)(97)	1334(53)(83)	1772(68)(110)	2190(86)(143)	3390(149)(239)
464	840(46)(89)	1248(58)(83)	1624(51)(91)	2045(89)(138)	3178(124)(206)
492	811(44)(82)	1246(46)(69)	1612(54)(92)	2018(75)(118)	3229(170)(299)

TABLE V. Fitted values for α and σ_0 for the form $\sigma=\sigma_0 A^\alpha$ for the mass dependence of the reaction and total cross sections measured in the present work. Also listed are total cross sections for π^- on free protons [23]. Cross sections are in mb.

		410 MeV	464 MeV	492 MeV
σ_R	σ_0	36.8(0.8)	34.06(0.98)	26.98(0.71)
	α	0.751(0.007)	0.765(0.008)	0.818(0.007)
σ_T	σ_0	38.2(1.4)	33.8(1.3)	30.7(1.3)
	α	0.853(0.010)	0.864(0.010)	0.881(0.010)
σ_T	(proton)	28.6	22.0	19.7

ties include the very small statistical uncertainty, the uncertainty of Monte Carlo corrections (included as a conservative value of about 1%), uncertainties in the elastic corrections arising from 0.5% differences found for the several optical model parameter sets explored, and the scatter among the methods used to extrapolate to zero solid angle. Uncertainties are larger for ^{6}Li and Ca because of the estimates needed for the contaminating heavier materials in these targets. All of the data are shown in Fig. 6 for the three beam energies used. We note that the data show very little dependence on the beam energy, and evolve smoothly with target mass.

An overall target mass dependence, from D through Pb, was obtained by fitting σ_R and σ_T to the form $\sigma=\sigma_0 A^\alpha$. Results are listed in Table V to summarize our observations. As the π^- beam energy increases, the free π^--p total cross section drops, as listed in Table V [23]. Corresponding decreases are seen in the fitted values of σ_0 for both reaction and total cross sections. The increased transparency to the beam at higher energies is also noted in the increasing values of the exponent.

The carbon target was used consistently in many determinations of reaction and total cross sections. Figure 7 shows the present results and the transmission results from Refs. [6–8]. Many differences can be found among the details of the methods, analyses and elastic corrections and methods of evaluating uncertainties, but the reaction cross sections seem to be highly robust. Another method to obtain reaction cross sections from data uses measured differential elastic scattering and a model to fit these data, then inferring σ_R from the same model. Data points in Fig. 7 show such results from Ref. [1]. These disagree strongly with transmission results, which are a more direct means to determine σ_R.

Total cross sections from transmission experiments on carbon shown in Fig. 7 also show good overall consistency, with some trend for the present experimental results to be somewhat below earlier data. The energy dependence of σ_T differs from that of σ_R because of the increase in elastic scattering due to the delta resonance just below this energy range. Total cross sections at 310 MeV and below are summarized in [21], demonstrating the persistence of this resonance in all but the heaviest nuclei. Points derived from the elastic scattering analysis [1] are again below the transmission data.

Total cross sections from the simple first-order Glauber model applied to other pion reactions from 400 to 500 MeV

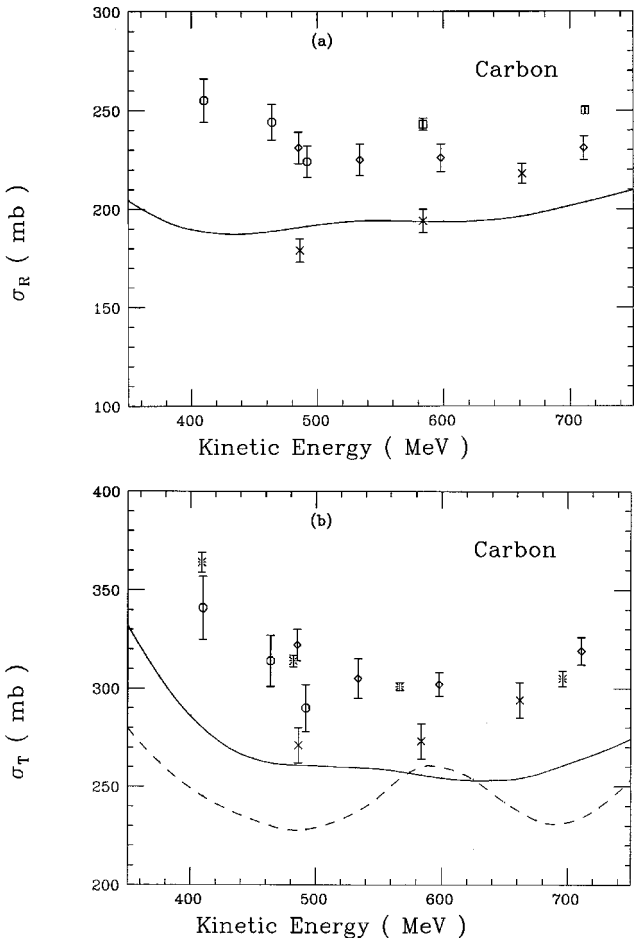

FIG. 7. Reaction and total cross sections for carbon from this work are shown as open circles, with those from the attenuation measurements of Ref. [6] as diamonds, Ref. [7] by stars, and Ref. [8] by squares. Crosses show results inferred from elastic scattering differential cross sections in Ref. [1]. The solid curves show the results of using the optical model of Ref. [5]. The dashed curve for total cross sections has been derived from scaling the free π^--nucleon total cross sections by the effective number of nucleons computed in the Glauber model of Ref. [22].

[22] are shown by the dashed curve in Fig. 7. No Fermi averaging has been applied. The edge of the delta resonance is seen at the left, and the $D_{13}(1520)$ is noted near a kinetic energy of 600 MeV. The data, even considering the different ways in which uncertainties are presented, show no such feature, even for a nucleus as light as carbon.

Figure 8 shows our data for σ_R with lead, compared to the transmission data from Ref. [8]. Problems of elastic corrections, plural scattering and extrapolations to zero solid angle are much more severe for this target. Our results are above the trend that might be deduced from the previous measurements, which extend to almost 1900 MeV.

The eikonal optical model [5] was used to compute reaction and total cross sections with the same input parameters as were used for the elastic corrections. Use of harmonic oscillator or Hartee-Fock distributions for carbon gave cross sections in agreement to within 1 mb, or 0.5% for σ_R and 0.35% for σ_T. These calculations are compared to the

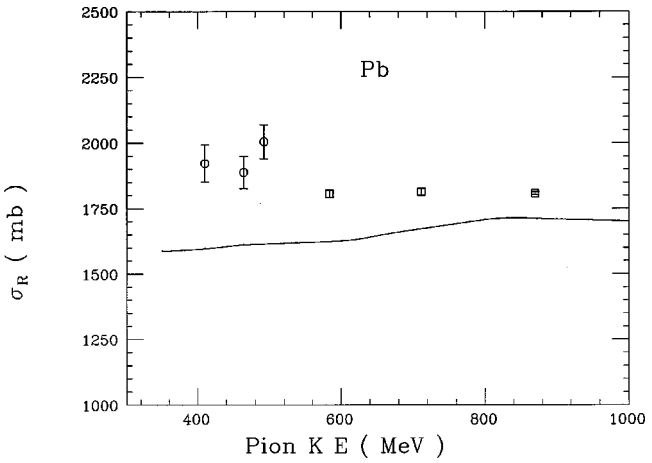

FIG. 8. Reaction cross sections from the present work for lead are compared to those from Ref. [8], shown by squares. The solid curve shows the values computed with the optical model of Ref. [5].

present and earlier results for carbon and lead in Figs. 7 and 8 as the solid curves. Pion-nucleon interactions have been Fermi averaged in this code. The shape of the energy dependences is similar to that of the carbon data for σ_R and for σ_T, but the magnitude of the predictions is low by about 40 mb for both. Since no pion absorption is included in this model, this reaction channel has not been included. The computed reaction and total cross sections use an optical model based on a sum of single scatterings and multiple scatterings, not including any explicit role of pion absorption, which needs two or more nucleons to occur. This process should then increase both σ_R and σ_T by the same amount above what we compute.

Measurements of $\sigma_{\rm abs}$ for 400 and 500 MeV π^+ give values of 38(17), 380(114), 415(105), and 590(148) mb for C, Zr, Sn, and Pb, respectively [24]. The differences between measured and computed reaction cross sections are less than measured absorption cross sections, not included in our computed values of σ_R, but not significantly, within mutual uncertainties.

The target mass dependence of computed σ_R and σ_T is shown in Fig. 6, at the central beam energy of 464 MeV. The same feature, with the data above the calculations, is found for all samples. Previous comparisons of measured and computed pion reaction cross sections have also found this same discrepancy at high energies [8].

The special case of ^{6}Li, with an average density less than half that of the other complex targets, was included in reference to the role of this nucleus for K^+ experiments [11]. When mass dependences fit for targets of carbon and heavier were used to compute ^{6}Li cross sections, those data are significantly below the trend extrapolated from above. Reaction cross sections measured for ^{6}Li are about 19 mb(13%) below that trend, and total cross sections are low by about 24 mb(15%). These comparisons could indicate a small density-dependent effect, seen in ^{6}Li, with about half the average density of carbon.

VI. CONCLUSIONS

Improvements in several techniques for determining π-nucleus total and reaction calculations have given results quite near earlier experiments. Reaction cross sections, in particular, seem to be highly robust observables. The present work, able to demonstrate for the first time that the model used for the important elastic corrections is valid, should yield results as good as the transmission method is able to provide.

In spite of agreement between eikonal [5] and other optical model [1,2] calculations and elastic data in many cases, the present work presents a significant and general disagreement for σ_T and σ_R, both being above calculated values, by amounts not far from measured absorption cross sections. Our computed elastic differential cross sections tend to lie below the data. If a means were found to increase those calculations, a corresponding decrease in ''measured'' σ_R and σ_T would ensue; this would worsen the comparison to absorption cross sections. Consistency might be achieved if the real part of the π-N interaction within nuclei were somewhat increased, enhancing the elastic differential calculations with little effect on computed σ_R and σ_T.

ACKNOWLEDGMENTS

This work was supported in part by the U.S. DOE. We are grateful to staff members at LAMPF for assistance during the run, and to H. Garzilazo for deuteron elastic calculations.

[1] T. Takahashi *et al.*, Phys. Rev. C **51**, 2542 (1995); T. Takahashi, Ph.D. thesis, Kyoto University, 1994.
[2] G. Kahrimanis *et al.*, Phys. Rev. C **55**, 2533 (1997).
[3] M.W. Rawool-Sullivan *et al.*, Phys. Rev. C **49**, 627 (1994).
[4] D. Marlow *et al.*, Phys. Rev. C **30**, 1662 (1984).
[5] C.M. Chen, D.J. Ernst, and M.J. Johnson, Phys. Rev. C **48**, 841 (1993).
[6] M. Crozon *et al.*, Nucl. Phys. **B64**, 567 (1965).
[7] A.S. Clough *et al.*, Nucl. Phys. **B76**, 15 (1974).
[8] B.W. Allardyce *et al.*, Nucl. Phys. **A209**, 1 (1973).
[9] C.M. Chen, D.J. Ernst, M.F. Jiang, and M.B. Johnson, Phys. Rev. C **52**, 485 (1995).
[10] C.M. Chen, M.B. Johnson, and D.J. Ernst, Phys. Rev. C **58**, 3500 (1998).
[11] E. Friedman *et al.*, Phys. Rev. C **55**, 1304 (1997).
[12] R.E. Chrien, R. Sawafta, R.J. Peterson, R.A. Michael, and E.V. Hungerford, Nucl. Phys. **A625**, 251 (1997).
[13] R.J. Peterson, Nucl. Phys. **A639**, 475 (1998).
[14] LAMPF Report No. LA-UR-87-327, Los Alamos National Laboratory, 1987.
[15] B.J. Kriss, Ph.D. thesis, University of Colorado, 1997.
[16] H. Garcilazo, Nucl. Phys. **A360**, 411 (1981); (private communication).
[17] O. Meirav *et al.*, Phys. Rev. C **40**, 843 (1989); **36**, 1066

(1987).
[18] W.B. Kaufman and W.R. Gibbs, Phys. Rev. C **40**, 1729 (1989).
[19] H. DeVries, C.W. DeJager, and C. DeVries, At. Data Nucl. Data Tables **36**, 495 (1987).
[20] J. Patterson and R. J. Peterson, University of Colorado Technical report, 1997 (unpublished).
[21] A.S. Carroll *et al.*, Phys. Rev. C **14**, 635 (1974).
[22] J. Ouyang, S. Hoibraten, and R.J. Peterson, Phys. Rev. C **47**, 2809 (1993).
[23] R.A. Arndt, I.I. Strakovsky, and R.L. Workman, Scattering Interactive Dial-In (SAID), available at URL http://clsaid.phys.vt.edu/~CAPS
[24] M.K. Jones *et al.*, Phys. Rev. C **48**, 2800 (1993).